Journal of Materials Chemistry A

PAPER

View Article Online
View Journal | View Issue

Cite this: J. Mater. Chem. A, 2017, 5, 19819

High energy Li-ion capacitors using two-dimensional $TiSe_{0.6}S_{1.4}$ as insertion host†

Apoorva Chaturvedi,[a] Peng Hu,[a] Christian Kloc,*[a] Yun-Sung Lee,[b] Vanchiappan Aravindan *[c] and Srinivasan Madhavi*[ad]

Received 22nd May 2017
Accepted 29th August 2017

DOI: 10.1039/c7ta04470d

rsc.li/materials-a

A remarkable improvement in energy density was found using Se-substituted two-dimensional TiS_2 ($TiSe_{0.6}S_{1.4}$) as the insertion matrix in a Li-ion capacitor (LIC) assembly with activated carbon (AC) as the counter electrode. Chemical vapor transport was successfully used to synthesize high quality $TiSe_{0.6}S_{1.4}$ with near-100% crystallinity and subsequently employed as a battery component in LICs. Prior to LIC fabrication, the Li-insertion properties were assessed in single-electrode configuration with metallic Li. Single-electrode performance is crucial for adjusting the mass loading of AC and $TiSe_{0.6}S_{1.4}$ to realize the maximum energy density. Accordingly, an AC/$TiSe_{0.6}S_{1.4}$-based LIC delivered an energy density of ~50 W h kg^{-1} with a good cyclability of 5000 cycles. Few undesirable side reactions with the electrolyte counterpart were observed for $TiSe_{0.6}S_{1.4}$, as supported by the impedance measurements.

Introduction

Recently, the fabrication of high-energy electrochemical energy storage devices without compromised power capabilities has been a popular research topic. Although Li-ion batteries (LIB) are capable of delivering high energies, they cannot translate the desired power, whereas supercapacitors, specifically electric double layer capacitors (EDLCs), are able to provide the necessary power, but have low energy densities.[1,2] Integration of both these energy storage systems into a single device would be an efficient approach to realizing both high energy and power capabilities. Amatucci *et al.*[3–6] reported the possibility of hybridizing insertion-type battery components as negative electrodes ($Li_4Ti_5O_{12}$) and supercapacitor-type electrodes (activated carbon, AC) as positive electrodes in the presence of aprotic organic solutions, called Li-ion capacitors (LICs).[7–11] Furthermore, LIC fabrication using aqueous solution is possible, but the decomposition potential of water results in operating limitations. Therefore, much research activity has been based on using organic solutions in practical configurations.[1,8,12] AC has been the unanimous choice as the EDLC component, irrespective of the assembly, and is responsible for boosting the power capability of the system owing to its high electrical conductivity and surface area, excellent chemical and electrochemical stability, low cost, and eco-friendliness.[13–17] This suggests that the increase in energy density is completely dependent on the development of high-performance insertion-type materials.

Among insertion-type materials exploited in prospective LICs, Ti-based materials, such as anatase and bronze phases of TiO_2, $Li_4Ti_5O_{12}$, $LiCrTiO_4$, TiP_2O_7, $TiNb_2O_7$, and $LiTi_2(PO_4)_3$, are appealing.[1,7,18–24] The high theoretical capacity (~175 mA h g^{-1}) and low insertion potential (~1.55 V *vs.* Li) of spinel $Li_4Ti_5O_{12}$ as a negative electrode has resulted in great progress toward the fabrication of commercial high-performance LICs in combination with AC. However, the energy density remains too low for high-end applications, such as electric vehicles and hybrid electric vehicles.[7,8,23] Therefore, research to develop existing $Li_4Ti_5O_{12}$ and explore new insertion-type materials has been greatly accelerated. Accordingly, we have attempted to explore the possibility of using two-dimensional (2D) titanium sulfoselenides (specifically, $TiSe_{0.6}S_{1.4}$) as an insertion matrix for the reversible accommodation of Li ions.[25–27] Employing 2D materials is among the best approaches for realizing perfect intercalation processes by utilizing the van der Waals gap between two adjacent layers. Furthermore, the higher theoretical capacity (~191 mA h g^{-1}) and single-phase reaction of these fascinating compounds is noteworthy.[26,28,29] Herein, a well-established chemical vapor transport (CVT) method is employed to prepare $TiSe_{0.6}S_{1.4}$ of the highest crystalline quality, which is subsequently employed as an insertion anode in combination with AC. Mass loading between the electrodes is optimized based on the half-cell performance with metallic Li prior to fabrication of the AC/$TiSe_{0.6}S_{1.4}$-based LIC. Necessary

[a]School of Materials Science and Engineering, Nanyang Technological University, Singapore 639798. E-mail: CKloc@ntu.edu.sg; Madhavi@ntu.edu.sg

[b]Faculty of Applied Chemical Engineering, Chonnam National University, Gwang-ju 500-757, Republic of Korea

[c]Department of Chemistry, Indian Institute of Science Education and Research (IISER), Tirupati-517507, India. E-mail: aravind_van@yahoo.com

[d]Energy Research Institute @ NTU (ERI@N), Nanyang Technological University, Singapore 637553

† Electronic supplementary information (ESI) available. See DOI: 10.1039/c7ta04470d

structural and electrochemical studies are performed and discussed in detail.

Experimental

$TiSe_{0.6}S_{1.4}$ crystalline bulk layered compounds were grown using CVT. Initially, pure titanium (99.9%, Alfa Aesar), sulfur powder (Puratronic, 99.999%, Alfa Aesar), and selenium shots (Alfa Aesar, 99.99%) were sealed in an evacuated quartz tube (10^{-5} Torr) with a small amount of iodine (I_2) added as a transport agent (2 mg cc^{-1}). The sealed ampoule (tube) was placed in a two-zone furnace with a temperature profile of 690–640 °C for a period of 14 days.[30] To prevent the ampoule exploding inside the furnace, the temperature was increased gradually (~5 K min^{-1}). The product was then carefully removed from the sealed ampule for further studies.

Secondary electron imaging (SEI) of the single crystal was performed using a SEM-JSM-6360 instrument (JEOL). Elemental distributions over crystal surfaces were studied using energy-dispersive X-ray (EDAX) analysis, which provided semi-quantitative compositional information. Corresponding elemental EDAX mapping of the synthesized sample was performed using the attached detector. Powder X-ray diffraction (P-XRD) data of single crystals were obtained with a Bruker D8 advance diffractometer (Cu Kα = 1.5406 Å radiation at 45 kV, 30 mA). Transmission electron microscopy (TEM) for selected area electron diffraction (SAED) was performed using JOEL HR-TEM 2010. Micro-Raman spectroscopy analysis was performed using WiTec Confocal Raman system (excitation wavelength, 532 nm; laser spot size, ~786 nm).

All electrochemical studies were performed in a CR2016 coin-cell assembly. Composite electrodes were formulated with 10 mg of active material (AC or $TiSe_{0.6}S_{1.4}$), 1 mg of conductive additive (Super P), and 1 mg of Teflonized acetylene black (TAB-2) as binder with ethanol. The slurry was placed over a 16 mm stainless steel mesh (Good Fellow, UK) and dried at 60 °C overnight before preparing test cells. Single-electrode and half-cell performances were studied using metallic Li as the counter and reference electrodes separated by Whatman paper (no. 1825-047). $LiPF_6$ (1 M) in ethylene carbonate and diethyl carbonate was used as the electrolyte. LICs were assembled using a fixed $TiSe_{0.6}S_{1.4}$ weight and adjusting the AC loading based on the half-cell performance with Li, while maintaining the aforementioned formulation. Galvanostatic studies were conducted at ambient temperature conditions (25 °C) using an Arbin BT2000 battery tester. Electrochemical impedance measurements were recorded on a Solartron 1470E instrument coupled with a frequency response analyzer.

Results and discussion

The P-XRD pattern confirmed the formation of a highly crystalline $TiSe_{0.6}S_{1.4}$ phase, showing sharp high-intensity diffraction peaks. The obtained P-XRD pattern is shown in Fig. 1a, in which all peaks belonged to the near-identical reported phase of $TiSe_{0.66}S_{1.34}$ ($P\bar{3}m1$), indexed to ICSD file no. 650871. The

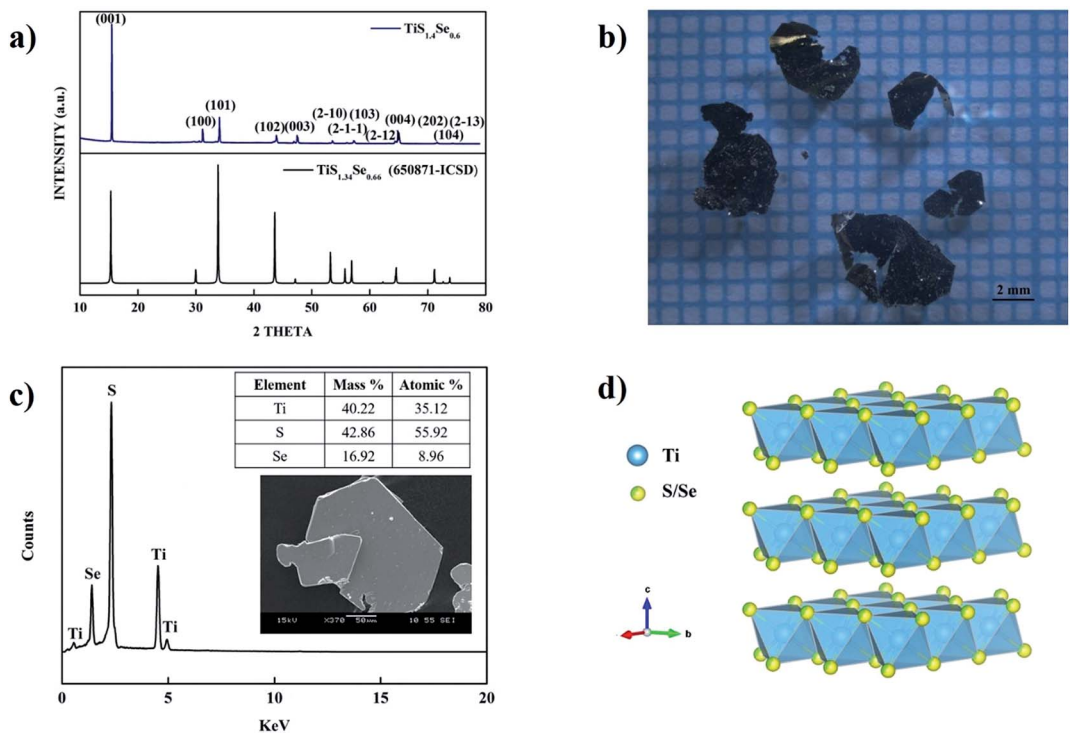

Fig. 1 (a) Powder X-ray diffraction pattern of as-grown $TiSe_{0.6}S_{1.4}$ indexed with standard ICSD file no. 650871 ($TiSe_{0.66}S_{1.34}$), (b) optical image of as-grown crystal flakes of $TiSe_{0.6}S_{1.4}$, (c) semi-quantitative analysis of as-grown $TiSe_{0.6}S_{1.4}$ crystallites, and (d) simulated crystal structure of $TiSe_{0.66}S_{1.34}$ (ICSD 650871) showing the layered compound morphology.

elemental composition of the synthesized phase was validated by X-ray fluorescence (Fig. S1†). The incorporation of bigger Se atoms in the lattice at S sites resulted in enhanced lattice parameters and inter-layer spacing in comparison with pristine TiS_2, as discussed in previous work.[26,30] $TiSe_{0.6}S_{1.4}$ crystalline flakes of micrometer-to-millimeter size were obtained using the method described above (Fig. 1b). A simulated structure of the above ICSD file was generated with the help of the VESTA 3.3 program, as shown in Fig. 1d, depicting the layered morphology of the synthesized compound that made it suitable for charge storage applications.

Initially, SEM/EDAX measurements were performed to investigate the semi-quantitative analysis of the prepared compound, as shown in Fig. 1. Fig. 1c shows a near-perfect stoichiometric ratio, indicating the purity of the product obtained. The homogeneous nature of the substitutional solid-solution compound was established by performing elemental EDAX mapping of a typical flake of the as-grown sample (Fig. 2). Raman spectroscopy study was also performed on the $TiSe_{0.6}S_{1.4}$ crystals to further establish the nature of the synthesized compound. The resulting spectrum was relatively similar to pristine TiS_2, with signals near the associated characteristic modes, such as E_g and A_{1g} positioned at ~233 and ~326 cm^{-1}, respectively.[31] The shift in the signal of A_{1g}-like mode and the emergence of an additional signal near the E_g-like mode were due to the presence of Ti/Se bonds in addition to Ti/S bonds, and are typical of such transition metal dichalcogenides.[32] To further determine the structure at atomic level, high resolution transmission electron microscopy (HR-TEM) data, including low magnification image, high resolution image, and select area electron diffraction (SAED), were collected and analyzed, confirming the hexagonal symmetry ($P\bar{3}m1$) of the atoms in the $TiSe_{0.6}S_{1.4}$ single crystal (Fig. 2c–e).[26,30]

Before constructing the high energy LIC, the optimal mass loading of the two electrodes components, namely the battery ($TiSe_{0.6}S_{1.4}$) and supercapacitor (AC), needed to be determined. The battery-type material underwent a perfect faradaic reaction during the charge–discharge process, while the supercapacitor component obeyed a double-layer formation across the electrode–electrolyte interface (accumulation of charge carriers over the AC surface). This clearly suggested the involvement of AC in a non-faradaic process.[1,25,33] The two different charge storage mechanisms in an LIC require the mass loading of AC and $TiSe_{0.6}S_{1.4}$ to be adjusted to maximize the energy density. Furthermore, the splitting of applied potential was dependent on the capability of the individual electrodes, irrespective of the storage mechanism.[34] As mentioned above, balancing the loadings of the electrodes enabled the maximum energy density to be realized. Therefore, half-cell/single-electrode studies were conducted for both AC and $TiSe_{0.6}S_{1.4}$ with metallic Li under

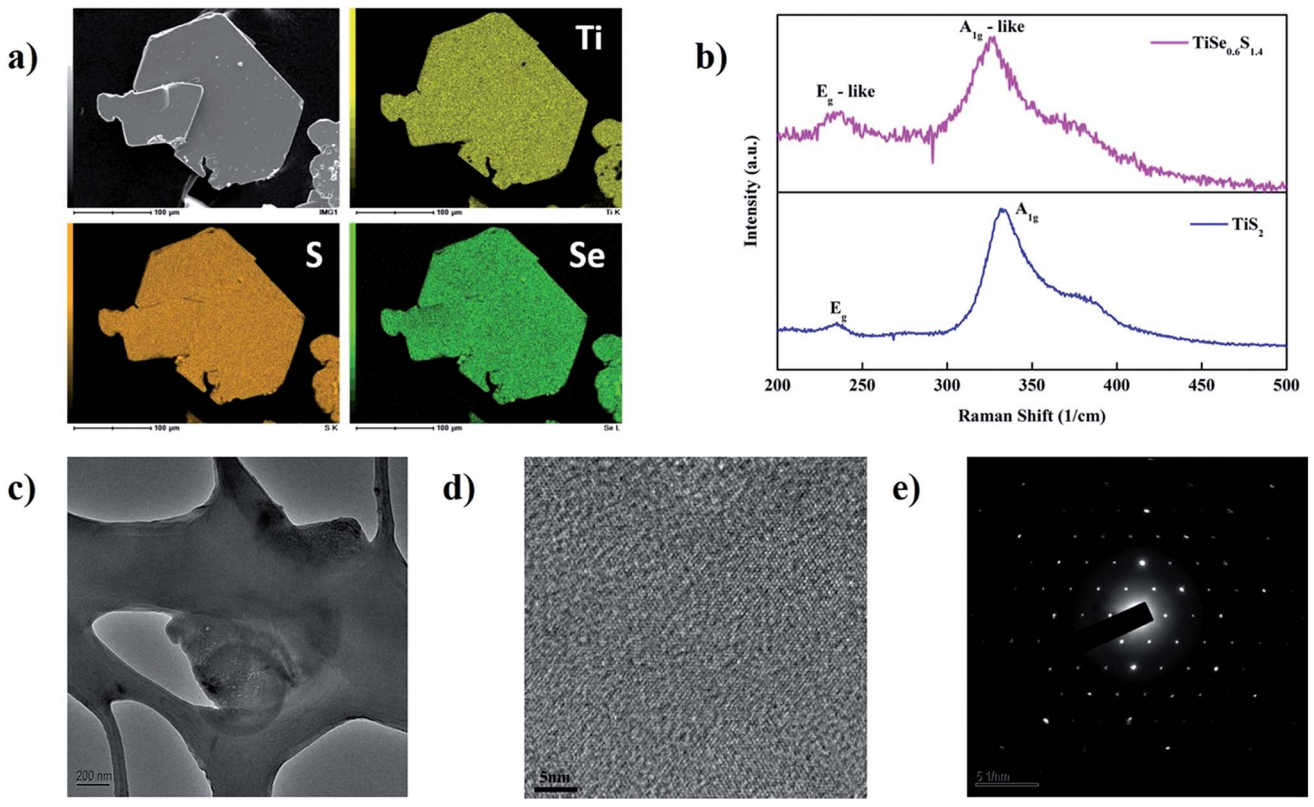

Fig. 2 (a) EDS elemental mapping of a typical as-synthesized crystalline flake of $TiSe_{0.6}S_{1.4}$, (b) Raman spectra of the Se-substituted compound ($TiSe_{0.6}S_{1.4}$) compared with that of pristine TiS_2, (c) low-resolution transmission electron microscopy image of the dispersed sample after sonication in ethanol, (d) corresponding high-resolution transmission electron microscopy image, and (e) selected area electron diffraction pattern.

a constant current density (such as 100 mA g^{-1}). As AC was procured from a commercial source (Kuraray, Japan), the Li/AC results were supplemented (Fig. S1†). The electrochemical activity of the Li/$TiSe_{0.6}S_{1.4}$ cell only is discussed in this section and is shown in Fig. 3. The cell displayed a Li-insertion capacity of ~161 mA h g^{-1}, which was ~84% of the theoretical capacity (~191 mA h g^{-1}). In contrast, the capacity of ~129 mA h g^{-1} was only reversed upon charging with a coulombic efficiency of ~80%. The irreversible capacity (~32 mA h g^{-1}) obtained from the first cycle was in line with the native compound, TiS_2, which exhibited an irreversible capacity of ~22 mA h g^{-1}.[28] Except for the first cycle, no irreversibility was observed and the cell showed excellent cycling stability. Furthermore, very high coulombic efficiency was registered in subsequent cycles (>99%). This clearly indicated that larger-sized Se substitution not only suppressed Li-intercalation in the van der Waals gap, but also diluted the efficiency in the first cycle. However, no reduction in Li insertion potential was noted and the presence of monotonous charge–discharge curves confirmed the single-phase reaction upon Li insertion/extraction.

Rate capability is another important factor for electrode materials in which mass loading of the active material plays a vital role. Therefore, a constant amount of active material was used in this study (10 mg), with the corresponding electrochemical profiles shown in Fig. 4. As expected, increasing the current rate tended to decrease the capacity. This was normal behavior because of partial utilization of the active material.[35] For instance, even at a high current rate of 600 mA g^{-1}, the cell produced a capacity of ~50 mA h g^{-1}. Interestingly, irrespective of the applied current rate, the Li/$TiSe_{0.6}S_{1.4}$ cell showed a high coulombic efficiency. This notable performance led us to fabricate the LIC with AC. Prior to this assembly, the anode

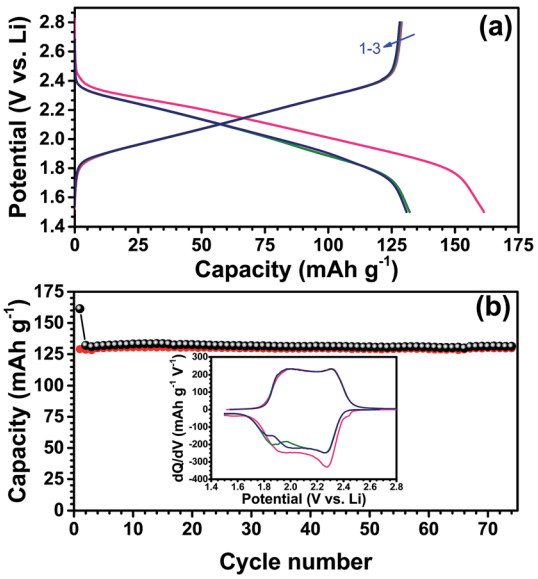

Fig. 3 (a) Electrochemical performance of Li/$TiSe_{0.6}S_{1.4}$ cell at 1.5–2.8 V *vs.* Li at a current density of 20 mA g^{-1}, and (b) plot of capacity *vs.* cycle number. Inset: differential capacity profiles of first three cycles in Fig. 2a. Active mass loading: 10 mg.

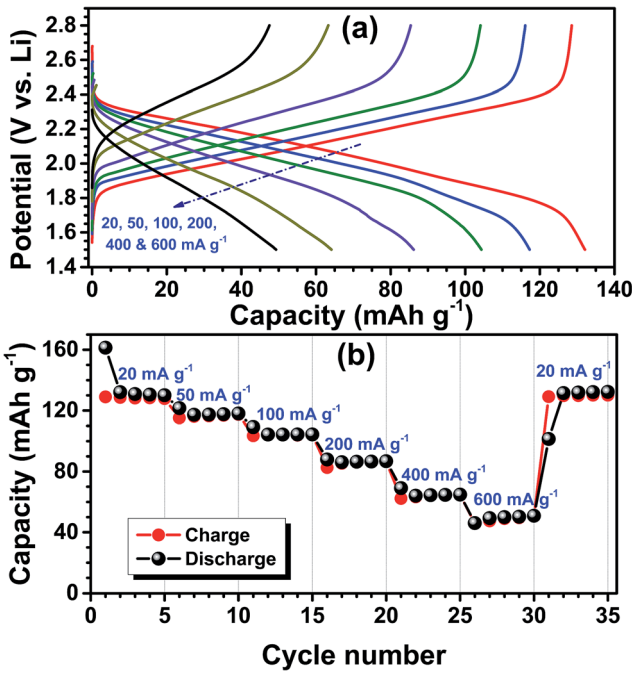

Fig. 4 (a) Typical charge–discharge curves of Li/$TiSe_{0.6}S_{1.4}$ cell between 1.5–2.8 V *vs.* Li at various current densities, and (b) plot of capacity *vs.* cycle number. Active mass loading: 10 mg.

($TiSe_{0.6}S_{1.4}$) to cathode (AC) loading had been fixed at a 1 : 2.8 ratio (5 mg : 14 mg), which was calculated from the half-cell performance of both materials with metallic Li under a constant current density (Fig. S2 and S3†).

AC/$TiSe_{0.6}S_{1.4}$-based LICs were fabricated in CR 2016 coin-cell assemblies with adjusted mass loadings, and the corresponding electrochemical profiles are shown in Fig. 5. As expected, increasing the applied current rate tended to decrease the discharge time. The applied current rate was calculated based on the active mass loading of both electrodes; for example, 1 A g^{-1} corresponded to 19 mA (total mass loading, 19 mg). Furthermore, the total mass loading was used to calculate the energy and power densities. Upon charging, Li ions present in the solution were intercalated in the $TiSe_{0.6}S_{1.4}$ lattice by obeying the faradaic reaction. On the counter electrode, the anions (PF_6^-) were attracted to the positive side, eventually forming an electric double layer across the electrode–electrolyte interface. This double layer formation not only boosted the power capability of the system, but also maintained charge neutrality in the solution. This process was reversed during discharge. Accordingly, the energy and power density values were calculated using the following equations:

$$P = \frac{i(\mathrm{A}) \times V}{m(\mathrm{mg}) \times 10^{-6}} \quad \text{and} \quad E = \frac{P \times \Delta t}{3600}$$

where i is the applied current (A), Δt is the discharge time (s), m is the total weight of active materials in both electrodes (19 mg), and V is the working potential of the cell measured at the intersection point of the charge–discharge curve at each current rate. The AC/$TiSe_{0.6}S_{1.4}$-based LIC delivered a maximum energy

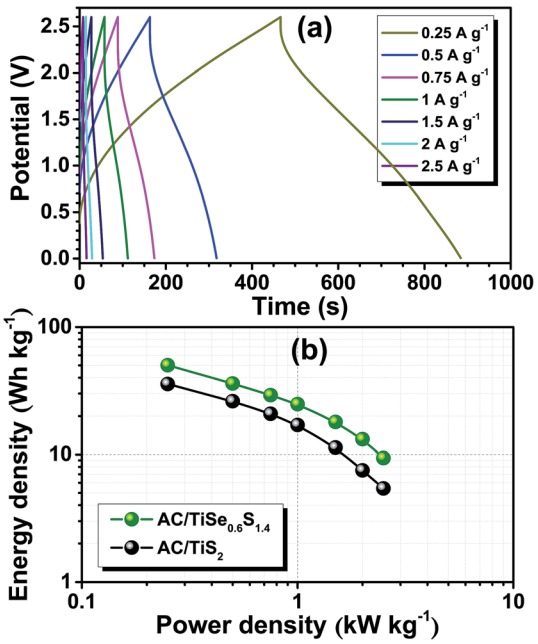

Fig. 5 (a) Typical charge–discharge curves of AC/$TiSe_{0.6}S_{1.4}$-based LIC at different current densities. Applied current density based on total mass loading (19 mg), and (b) Ragone plot of AC/$TiSe_{0.6}S_{1.4}$-based LIC compared with the AC/TiS_2 system.

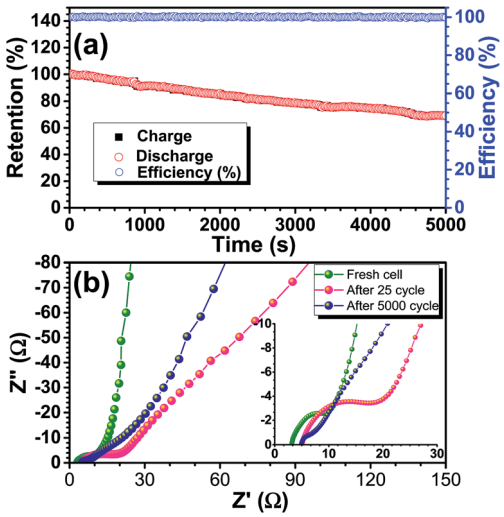

Fig. 6 (a) Galvanostatic cycling profiles of AC/$TiSe_{0.6}S_{1.4}$-based LIC cycles at current density of 1 A g^{-1} with coulombic efficiency, assuming an energy density of ~25 W h kg^{-1} at 100%, and (b) electrochemical impedance spectra of the AC/$TiSe_{0.6}S_{1.4}$ cell recorded at different intervals.

density of ~50 W h kg^{-1}, which was ~14 W h kg^{-1} higher than the parent compound in a similar setup (AC/TiS_2).[28] This represented ~40 and ~73% improvements in these values when applying lower and high power rates compared with the TiS_2-based LIC. This remarkable enhancement was mainly due to partial substitution of Se. This partial substitution increased the interlayer spacing between the two adjacent $TiSe_{0.6}S_{1.4}$ layers, which weakened the van der Waals forces between the layers. This eventually led to a facile Li-insertion/extraction process and promoted the energy density of the system compared to the native system (TiS_2), especially at higher power rates. Furthermore, the AC/$TiSe_{0.6}S_{1.4}$-based LIC displayed much better electrochemical storage behavior than other systems, such as TiS_2,[28] TiO_2–B[21], $Li_3V_2(PO_4)_3$,[36] and $LiNi_{0.5}Mn_{1.5}O_4$ (octahedral sites)[37] with AC as the counter electrode (Fig. S4†). Although Se substitution suppressed the reversibility compared to TiS_2, the overall AC/$TiSe_{0.6}S_{1.4}$-based LIC performance was found to be appealing. As noted above, at higher power rates, the energy density declined owing to partial utilization of the active materials. This AC/$TiSe_{0.6}S_{1.4}$ system even displayed much better performance than the commercial AC/$Li_4Ti_5O_{12}$ system.[1] However, power density was an issue in the AC/$TiSe_{0.6}S_{1.4}$ system, but can be easily tackled by adopting carbon coating, or formulating composites of carbonaceous materials, such as graphene, AC, and carbon nanotubes, and battery-type components, or modifying AC with surface functionalization, such as heteroatom doping and tailoring micro/mesoporosity.

Cyclability is another crucial factor when studying the possibility of practical applications. Accordingly, AC/$TiSe_{0.6}S_{1.4}$-based LIC was subjected to a high current cycling (1 A g^{-1}) and the corresponding coulombic efficiency is shown in Fig. 6. The energy density at 1 A g^{-1} was normalized to 100% and the cycling profiles were calculated accordingly. A decrease in energy density was noted upon cycling; for example, ~69% (~17 W h kg^{-1}) of the density was retained after 5000 cycles. Although, this decrease was slightly larger for the AC/$TiSe_{0.6}S_{1.4}$-based LIC, the delivery was much better than the TiS_2-based LIC,[28] in which ~75% retention was noted after 2000 cycles, while ~85% retention was found in the AC/$TiSe_{0.6}S_{1.4}$ system. It has been well established that the formulation of composites with carbonaceous counterparts not only improves the power capability of the system, but also improves the capacity retention characteristics. The same strategy could be applied to further improve the cyclability of LIC, as our main goal was to maximize the energy density of these fascinating 2D dichalcogenides, preferably TiS_2-based compounds, to obtain commercially applicable materials without compromising the cyclability.[32] EIS spectra of the AC/$TiSe_{0.6}S_{1.4}$-based LIC are shown in Fig. 6b. The Nyquist plot was composed of three main regions, with the high-frequency region likely associated with solution resistance, the medium-frequency region related to the charge-transfer (R_{CT}) properties, and the vertical tail (Warburg tail) attributed to the diffusion controlled process. The increase in cell impedance (R_{CT}) was mainly associated with the formation of a poor Li phase *via* irreversible consumption during the first discharge. The rich Li phase started forming and a decline in the R_{CT} values was recorded, which was highly conductive and formed *via* the slower accumulation of the desired Li ions with extended cycling. Marginal increments in R_{CT} were noted for AC/$TiSe_{0.6}S_{1.4}$-based LICs, even after 5000 cycles, in contrast to AC/TiS_2. This clearly suggests that the battery-type component was not involved in the undesirable side reaction with the electrolyte solution. This is an important advantage of this kind

of 2D material. Studies toward improving the energy density and retention characteristics are in progress to continue progressing this material to be commercially viable without compromising the power capability.

Conclusion

We successfully demonstrated the possibility of using Se-substituted TiS_2 as promising insertion hosts for reversible accommodation in Li ions for Li ion capacitors assembled with AC as the counter electrode. The AC/$TiSe_{0.6}S_{1.4}$-based LICs delivered a maximum energy density of $\sim$50 W h kg^{-1} and satisfactory cycling profiles. Furthermore, the AC/$TiSe_{0.6}S_{1.4}$ cell, in particular, the battery-type component, exhibited excellent all-round characteristics, including energy density, cyclability, and low unwanted reactivity with the electrolyte, compared with its native phase, TiS_2. We believe that Se substitution is a major reason for these enhancements. Further studies are in progress to improve the performance to make the system commercially viable.

Conflicts of interest

There are no conflicts to declare.

Acknowledgements

This work was financially supported by NTU-HUJ Create Phase II, a joint research program between the Hebrew University of Jerusalem (HUJ, Israel) and Nanyang Technological University (NTU, Singapore) with CREATE (Campus for Research Excellence and Technological Enterprise) funding from the National Research Foundation of Singapore (NRF, Singapore). VA is grateful for financial support from the Science & Engineering Research Board (SERB), a statutory body of the Department of Science & Technology, Govt. of India through a Ramanujan Fellowship (SB/S2/RJN-088/2016).

References

1 V. Aravindan, J. Gnanaraj, Y.-S. Lee and S. Madhavi, *Chem. Rev.*, 2014, **114**, 11619–11635.
2 V. Aravindan, Y.-S. Lee and S. Madhavi, *Adv. Energy Mater.*, 2015, **5**, 1402225.
3 I. Plitz, A. DuPasquier, F. Badway, J. Gural, N. Pereira, A. Gmitter and G. G. Amatucci, *Appl. Phys. A: Mater. Sci. Process.*, 2006, **82**, 615–626.
4 A. Du Pasquier, I. Plitz, S. Menocal and G. Amatucci, *J. Power Sources*, 2003, **115**, 171–178.
5 A. D. Pasquier, I. Plitz, J. Gural, F. Badway and G. G. Amatucci, *J. Power Sources*, 2004, **136**, 160–170.
6 G. G. Amatucci, F. Badway, A. Du Pasquier and T. Zheng, *J. Electrochem. Soc.*, 2001, **148**, A930–A939.
7 K. Naoi, W. Naoi, S. Aoyagi, J.-i. Miyamoto and T. Kamino, *Acc. Chem. Res.*, 2013, **46**, 1075–1083.
8 K. Naoi, S. Ishimoto, J.-i. Miyamoto and W. Naoi, *Energy Environ. Sci.*, 2012, **5**, 9363–9373.
9 K. Naoi and Y. Nagano, in *Supercapacitors*, Wiley-VCH Verlag GmbH & Co, KGaA, Weinheim, Germany, 2013, DOI: 10.1002/9783527646661.ch7, pp. 239–256.
10 M. Yang and Z. Zhou, *Adv. Sci.*, 2017, 201600408.
11 M. Yang, Y. Zhong, J. Ren, X. Zhou, J. Wei and Z. Zhou, *Adv. Energy Mater.*, 2015, **5**, 1500550.
12 J. J. Ren, L. W. Su, X. Qin, M. Yang, J. P. Wei, Z. Zhou and P. W. Shen, *J. Power Sources*, 2014, **264**, 108–113.
13 T. Brousse, D. Bélanger and D. Guay, in *Supercapacitors*, Wiley-VCH Verlag GmbH & Co, KGaA, Weinheim, Germany, 2013, DOI: 10.1002/9783527646661.ch8, pp. 257–288.
14 A. G. Pandolfo and A. F. Hollenkamp, *J. Power Sources*, 2006, **157**, 11–27.
15 E. Frackowiak, *Phys. Chem. Chem. Phys.*, 2007, **9**, 1774–1785.
16 J. Zhang, M. Terrones, C. R. Park, R. Mukherjee, M. Monthioux, N. Koratkar, Y. S. Kim, R. Hurt, E. Frackowiak, T. Enoki, Y. Chen, Y. Chen and A. Bianco, *Carbon*, 2016, **98**, 708–732.
17 Y. Gogotsi, *MRS Bull.*, 2015, **40**, 1110–1121.
18 V. Aravindan, M. V. Reddy, S. Madhavi, S. G. Mhaisalkar, G. V. Subba Rao and B. V. R. Chowdari, *J. Power Sources*, 2011, **196**, 8850–8854.
19 V. Aravindan, W. Chuiling and S. Madhavi, *J. Mater. Chem.*, 2012, **22**, 16026–16031.
20 V. Aravindan, W. Chuiling, M. V. Reddy, G. V. S. Rao, B. V. R. Chowdari and S. Madhavi, *Phys. Chem. Chem. Phys.*, 2012, **14**, 5808–5814.
21 V. Aravindan, N. Shubha, W. C. Ling and S. Madhavi, *J. Mater. Chem. A*, 2013, **1**, 6145–6151.
22 V. Aravindan, J. Sundaramurthy, A. Jain, P. S. Kumar, W. C. Ling, S. Ramakrishna, M. P. Srinivasan and S. Madhavi, *ChemSusChem*, 2014, **7**, 1858–1863.
23 K. Naoi, S. Ishimoto, Y. Isobe and S. Aoyagi, *J. Power Sources*, 2010, **195**, 6250–6254.
24 H.-K. Kim, D. Mhamane, M.-S. Kim, H.-K. Roh, V. Aravindan, S. Madhavi, K. C. Roh and K.-B. Kim, *J. Power Sources*, 2016, **327**, 171–177.
25 M. R. Lukatskaya, B. Dunn and Y. Gogotsi, *Nat. Commun.*, 2016, **7**, 12647.
26 S. Kikkawa, H. Ohkura and M. Koizumi, *Mater. Res. Bull.*, 1987, **22**, 1337–1340.
27 C. Tan and H. Zhang, *Chem. Soc. Rev.*, 2015, **44**, 2713–2731.
28 A. Chaturvedi, P. Hu, V. Aravindan, C. Kloc and S. Madhavi, *J. Mater. Chem. A*, 2017, **5**, 9177–9181.
29 R. Elazari, G. Salitra, G. Gershinsky, A. Garsuch, A. Panchenko and D. Aurbach, *J. Electrochem. Soc.*, 2012, **159**, A1440–A1445.
30 H. P. B. Rimmington, A. A. Balchin and B. K. Tanner, *J. Cryst. Growth*, 1972, **15**, 51–56.
31 D. Y. Oh, Y. E. Choi, D. H. Kim, Y.-G. Lee, B.-S. Kim, J. Park, H. Sohn and Y. S. Jung, *J. Mater. Chem. A*, 2016, **4**, 10329–10335.
32 L. M. Xie, *Nanoscale*, 2015, **7**, 18392–18401.
33 V. Aravindan, M. Ulaganathan and S. Madhavi, *J. Mater. Chem. A*, 2016, **4**, 7538–7548.

34 V. Khomenko, E. Raymundo-Pinero and F. Beguin, *J. Power Sources*, 2006, **153**, 183–190.
35 K. Zaghib, J. B. Goodenough, A. Mauger and C. Julien, *J. Power Sources*, 2009, **194**, 1021–1023.
36 R. Satish, V. Aravindan, W. C. Ling and S. Madhavi, *J. Power Sources*, 2015, **281**, 310–317.
37 N. Arun, A. Jain, V. Aravindan, S. Jayaraman, W. Chui Ling, M. P. Srinivasan and S. Madhavi, *Nano Energy*, 2015, **12**, 69–75.